Collective structural relaxation in phase-change memory devices

Manuel Le Gallo*,[1, a)] Daniel Krebs,[1] Federico Zipoli,[1] Martin Salinga,[1, 2] and Abu Sebastian*[1, b)]
[1)] *IBM Research – Zurich, 8803 Rüschlikon, Switzerland.*
[2)] *RWTH Aachen, 52074 Aachen, Germany*

Phase-change memory devices are expected to play a key role in future computing systems as both memory and computing elements. A key challenge in this respect is the temporal evolution of the resistance levels commonly referred to as "resistance drift". In this paper, we present a comprehensive description of resistance drift as a result of spontaneous structural relaxation of the amorphous phase-change material towards an energetically more favorable ideal glass state. Molecular dynamics simulations provide insights into the microscopic origin of the structural relaxation. Based on those insights, a collective relaxation model is proposed to capture the kinetics of structural relaxation. By linking the physical material parameters governing electrical transport to such a description of structural relaxation, we obtain an integrated drift model that is able to predict the current-voltage characteristics at any instance in time even during non-trivial temperature treatments. We demonstrate accurate quantitative matching with experimental drift measurements over a wide range of time (10 decades) and temperature (160 - 420 K).

I. INTRODUCTION

Phase-change memory (PCM) is arguably the most advanced resistive memory technology[1,2]. A PCM device consists of nanometric volumes of phase-change materials such as $Ge_2Sb_2Te_5$[3,4]. The phase-change material can be rapidly and reversibly switched between the amorphous and crystalline states, leading to a significant change in its electrical properties. The resistivity of the two phases differs by orders of magnitude, opening the possibility to use the device to store information. It is also possible to achieve a continuum of resistance levels by varying the ratio of crystalline/amorphous fractions. This enables multi-bit storage, allowing the increase of the memory capacity of a single PCM device[5,6]. This near-analog storage capability is also appealing for emerging applications in non-von Neumann computing such as computational memory[7–11]. It also facilitates applications in brain-inspired neuromorphic computing where PCM devices are used to emulate synaptic and neuronal behavior[12–14]. A key challenge in all these application domains is the temporal evolution of resistance levels commonly referred to as resistance drift[15]. These resistance variations are caused mostly by the phase-change material in the amorphous phase. At constant ambient temperature, the resistance typically exhibits a temporal dependence characterized by

$$R(t) = R(t_0)(t/t_0)^{\nu_R}, \text{ or equivalently } \log(R(t)/R(t_0)) = \nu_R \log(t/t_0) \tag{1}$$

where $R(t_0)$ is the resistance measured at time t_0 and ν_R is the so-called drift exponent. There is wide consensus that resistance drift is caused by the spontaneous structural relaxation of the amorphous phase-change material[16–19]. In a PCM device, to induce the crystalline-amorphous phase transition, the phase-change material is melted and rapidly quenched. This creates a low-ordered highly-stressed amorphous state. Over time, this amorphous state evolves towards an energetically more favorable "ideal glass" state.

In this article, we present a comprehensive description of resistance drift based on a review and integration of several recent findings that have been published over the last few years[20–23]. This manuscript aims at integrating all the relevant data and modeling efforts that were previously published in a unified manner, and includes significant additional explanations, discussions, and context to the research that was performed. We start with a peak into the microscopic origins of structural relaxation by reviewing recent insights from first-principles calculations. Next, we present a collective relaxation model that captures the kinetics of this structural relaxation. It is shown that such a model naturally gives rise to the characteristic logarithmic evolution in time. By linking material parameters governing the electrical transport to such relaxation, we can consistently capture the evolution of the current-voltage (I–V) behavior of PCM devices over time and temperature.

II. MICROSCOPIC ORIGIN OF STRUCTURAL RELAXATION

Recent first-principles calculations by Raty et al.[25], Gabardi et al.[26], and Zipoli et al.[22] on the prototypical phase-change material GeTe provide significant insights into the microscopic picture of structural relaxation and nature of the "ideal glass". To identify the structural roots of resistance drift, the structures responsible for localized states in the band gap for melt-quenched

[a)] Electronic mail: anu@zurich.ibm.com
[b)] Electronic mail: ase@zurich.ibm.com

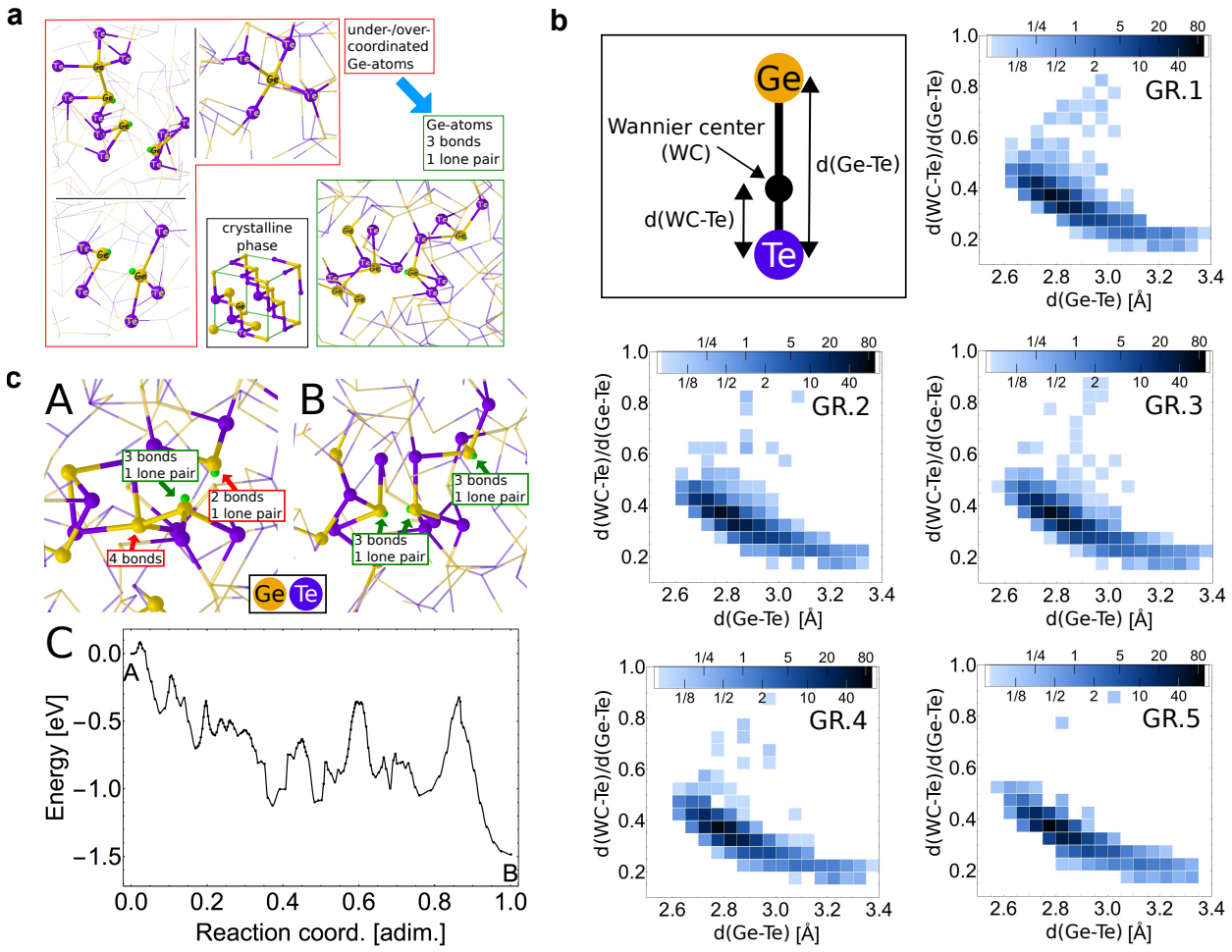

FIG. 1. **Structural relaxation in amorphous GeTe a** Examples of structures with Ge atoms having a bond configuration different from the ideal chemically ordered three-fold one are illustrated within the red contour. Such structures are responsible for localized electronic states in the band gap. Recent studies show that resistance drift is mostly caused by a gradual transition of these structures formed during the melt-quench process towards lower energy structures having more ideal configurations. The green box shows an example of an amorphous region consisting of Ge atoms with three-fold bond configurations. Ge and Te atoms are depicted as dark yellow and violet spheres, respectively. Bonds between these atoms, determined using Wannier analysis[22,24] are indicated by cylinders and the surrounding bond network via thin lines. **b** The link between distribution of bond configurations and conductivity is shown here. Each histogram shows the distribution of bond configurations of all the Ge-Te bonds characterized by bond polarization and bond distance. Sixty-five structures obtained via classical MD simulations and analyzed via first-principles calculations are grouped into five sets ranging from high conductivity (GR.1) to low conductivity (GR.5), see Ref. 22 for more details. The number of bonds in each bin normalized by the number of configurations of the group is indicated by the color scale. Amorphous states with a higher conductivity show a broader distribution. Upon relaxation, i.e. with decreasing conductivity, the distribution of Ge-Te bonds becomes sharper and outliers disappear. **c** The energy profile associated with the annealing of a defective Ge-Te structure is shown. The starting condition (Panel A) produces an electronic state in the band gap. In the final state (Panel B), i.e. after the annealing, the defective configurations causing the localized electronic state are removed. Red arrows indicate the Ge atoms with defective configurations. Green arrows indicate Ge atoms with an ideal three-fold bond configuration. The minimum energy pathway at $T = 0\,\mathrm{K}$ (Panel C) shows that the process occurs via a complex sequence of activated processes characterized by a changing collective activation energy. Adapted from Ref. 22.

amorphous GeTe were carefully analyzed. It was found that they consist of groups of Ge atoms close to each other in which the coordination of at least one Ge atom differs from a threefold coordination with only Te atoms as nearest neighbors as shown in Figure 1**a**[22,27]. Resistance drift is associated with a transition of these structural defects into lower-energy structures having a chemically ordered three-fold bonding topology and to a removal of stretched bonds in the amorphous network. The role of stretched and compressed bonds is further analyzed in Figure 1**b** by plotting the correlation between conductivity and distribution of Ge-Te bond lengths. The histograms of normalized bond polarizations and bond distances show that an increase of resistance

is linked to the topology of a-GeTe tending towards less stretched and compressed Ge-Te bonds with a distance of approximately 2.8 Å and bond polarization of 0.35 (moving from conductivity groups GR.1 to GR.5). Structures with more bonds deviating significantly from this configuration especially with respect to the bond polarization were found to be more conductive.

Figure 1**c** illustrates the energy profile associated with the reactive pathways to relax a group of three Ge atoms, two of which with coordination differing from the chemically ordered three-fold bonding topology. The plot of energy versus reaction coordinate shows that the annihilation of this defect results in a lower energy configuration with all three Ge atoms having the ideal bonding configuration. The electron state localized in the band gap associated with this defect is not present in the final configuration anymore. Unfortunately, due to the poor statistics, it is not possible to derive a distribution of activation energy barriers from those simulations. The energy profile in Figure 1**c** illustrates that a variety of activation energy barriers are overcome in the process of structural relaxation of amorphous GeTe.

Although the studies described in Refs. 22, 25, and 26 have some differences, they seem to agree that drift in amorphous GeTe manifests in the annihilation of defects comprising groups of Ge atoms in which the coordination of at least one Ge atom differs from that of the ideal three-fold bonding configuration. An increase in resistance is correlated with the annihilation of these defects accompanied by a slow evolution of the bond network towards more ideal bonding configurations. While the change in electronic band structure due to relaxation is still under debate[22,25,28], it is commonly accepted that the resistance increase results from an increase of the activation energy for conduction upon relaxation.

III. KINETICS OF STRUCTURAL RELAXATION: CURRENT UNDERSTANDING AND SHORTCOMINGS

The kinetics of structural relaxation in phase-change materials are to-date mostly described by a two-state model for the relaxation of defects[29,30]. This is based on the popular relaxation model proposed by Gibbs[31]. The essential idea is that there are structural defects that can be removed by relaxation. Different activation energies are required to remove different defects assuming that the removal of one defect can be associated with a single activation energy. As the relaxation proceeds, defects with lower activation energy will be removed first, followed by those with higher activation energy. The distribution of activation energies for the relaxation of defects serves as the parameter that tracks the state of relaxation of the material at any instance in time.

If we denote $q(E)$ the distribution of activation energies for relaxation, mono-molecular[32] relaxation can be described by

$$\frac{\mathrm{d}q(E)}{\mathrm{d}t} = -\nu(E)q(E) \tag{2}$$

where the relaxation rate $\nu(E)$ has an Arrhenius-type temperature dependence with activation energy E

$$\nu(E) = \nu_0 \exp(-E/k_\mathrm{B}T).$$

ν_0 is the attempt to relax frequency on the order of typical phonon frequencies, k_B is the Boltzmann constant and T is the temperature.

Following (2), the structural defects with low activation energies relax first. Thus, over time relaxation becomes gradually more difficult as the number of unrelaxed defects decreases and the average activation energy of the remaining structural defects increases. The mathematical problem therefore comes down to counting the number of structural defects that remain to relax in order to describe the state of relaxation of the system.

Integration over Eq. (2) yields

$$\int_{q_0(E)}^{q(E,t)} \frac{\mathrm{d}q}{q} = -\int_0^t \nu_0 \exp\left(-\frac{E}{k_\mathrm{B}T}\right) \mathrm{d}\tau,$$

and can be solved analytically for constant temperature

$$q(E,t) = q_0(E)\exp(-t\nu_0 \exp(-E/k_\mathrm{B}T)).$$

For $t > 1/\nu_0$ the term $\exp(-t\nu_0\exp(-E/k_\mathrm{B}T))$ can be approximated by a step function $\theta(E-E_0)$ with $E_0 = k_\mathrm{B}T\log(\nu_0 t)$.

Finally, the number of remaining unrelaxed structural defects can be derived by integrating over all activation energies that have not undergone relaxation until time t. Assuming that $q_0(E)$ is uniformly distributed from 0 to an energy E_{max}, for $0 < E_0 < E_{max}$ a $\log(t)$ dependence emerges

$$q(t) = \int q(E,t)\mathrm{d}E \approx \int_{E_0}^{E_{max}} \frac{1}{E_{max}}\mathrm{d}E = 1 - \frac{k_\mathrm{B}T}{E_{max}}\log(\nu_0 t). \tag{3}$$

Even though this model is quite appealing, it has a few drawbacks. To quantitatively capture the commonly measured $\log(t)$ drift behavior in phase-change materials, it is necessary to have a flat distribution of activation energies[29] as indicated by Eq.

(3). Since the $\log(t)$ kinetics have been observed over a wide range of time (from $\sim 100\,\mathrm{ns}$[33] up to months) and temperature, the energy range over which $q_0(E)$ is uniform would need to be quite large (presumably $> 0.8\,\mathrm{eV}$, assuming a drift timescale of $10^{-7}\,\mathrm{s}$ to $10^{7}\,\mathrm{s}$ at room temperature). Given the universality of the drift behavior in phase-change materials, this strict requirement on the energetic distribution irrespective of the material used seems unnatural. A further concern is that in this picture, the defects that have undergone relaxation once, no longer participate in subsequent structural relaxation processes. Finally, this picture also does not account for the fact that a local rearrangement inherently influences also the surroundings, which will more or less subtly rearrange as well.

The molecular dynamics simulations described in Section II have shed light onto the relaxation of the complex structures with defective local coordination present in amorphous phase-change materials. As shown in Figure 1**c**, it is observed that relaxation leading to the annihilation of a particular defective structural complex occurs via a series of collective rearrangements, whereby individual local configurations are changed many times. Hence, an overall lower energy state is achieved through the repeated involvement of many atoms rather than by a very local defect relaxing once and not changing afterwards again. In contrast, Gibbs approach assumes that the removal of one defect is associated with a single activation energy, and it is the distribution of activation energies associated to the spectrum of defects that determines the state of relaxation of the material. The collective relaxation model presented in the next section provides an alternative to the Gibbs approach without the drawbacks mentioned above.

IV. COLLECTIVE RELAXATION MODEL

Most approaches to describe the evolution of a macroscopic property that is logarithmic in time, including the defect relaxation model by Gibbs et al.[31], argue with the microscopic inhomogeneity in the relaxing material to justify the very specific distribution of activation energies of the relaxation processes that is necessary to yield the log-law. Already in 1948, Kuhlmann commented that this seems rather forced as so many different materials show the very same relaxation behavior[34]. Kuhlmann argued instead, that the empirical log-law $x = \frac{k_\mathrm{B}T}{A}\log(Bt)$ for a property x changing with time t would arise naturally without any further assumptions if structural relaxation occurs via a large number of statistical processes with an activation energy that depends linearly on the relaxing property as described by

$$\frac{\mathrm{d}x}{\mathrm{d}t} = \frac{k_\mathrm{B}T}{A}\exp\left(-\frac{Ax}{k_\mathrm{B}T}\right)B.$$

This argument is not only mathematically simple but also seems to be naturally built into any glass-system. A glass is formed when it is cooled down from the melt faster than it can sample all possible structural configurations in the energy-landscape. At this point, it forms a non-equilibrium structure that naturally has built-in stresses. As the glass is globally relaxing towards its ideal state, those stresses relax through localized reconfigurations and the local configurations become more stabilized. A group of atoms neighboring a region that previously relaxed needs for their own relaxation to partially involve those stabilized atoms from that already relaxed region. Hence, for this subsequent relaxation a higher activation energy must be overcome.

The collective relaxation model based on this physical picture is motivated by a similar relaxation problem encountered in the study of indents created in a polymer film using a heated atomic force microscopy probe[35]. The essential idea is that the atomic configurations that are frozen in during the glass transition relax collectively towards the more energetically favorable "ideal glass" state. The relaxation proceeds in a sequence of transitions between neighboring unrelaxed amorphous states. The driving force for such a relaxation is the difference between the local energy minima of two neighboring states, denoted Δ_b. The closer to equilibrium the system is, the lower will be the driving force and the higher the energy barrier for subsequent relaxation (see Figure 2). The rates of the relaxation events in the direction towards equilibrium n^- and in the opposite direction n^+ are then given by

$$n^- = \nu_0 \exp\left(-\frac{E_b}{k_\mathrm{B}T}\right)$$
$$n^+ = \nu_0 \exp\left(-\frac{E_b+\Delta_b}{k_\mathrm{B}T}\right)$$

where ν_0 is an attempt-to-relax frequency and E_b is the energy barrier for subsequent relaxation events. We denote by Σ the distance of the unrelaxed state from the "ideal glass" state. Σ takes values between 0 and 1, with 1 denoting the fully unrelaxed state and 0 the "ideal glass" state[21,23]. If each relaxation event changes Σ by an amount Δ_Σ, the evolution of Σ is then given by

$$\frac{\mathrm{d}\Sigma}{\mathrm{d}t} = \Delta_\Sigma(n^+ - n^-).$$

The amorphous state is assumed to be created with an initial distance $\Sigma(0) = \Sigma_0$ from equilibrium. After each relaxation event, the system reaches structures lower in energy as stress is relaxed and the driving force Δ_b reduces. Therefore, the activation

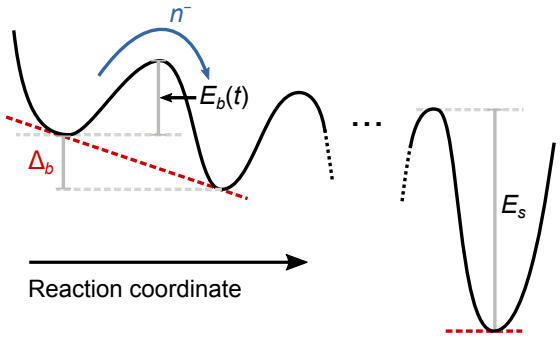

FIG. 2. **Sketch of the collective relaxation model** The amorphous state created via the melt-quench process is in an unstable state and proceeds through a sequence of transitions towards the energetically more favorable "ideal glass" state. The activation energy $E_b(t)$ for collective reconfigurations grows as they involve the movement of atoms that have been increasingly stabilized in their positions through previous relaxation steps.

energy E_b for relaxation events increases monotonically upon approaching equilibrium until it reaches its highest value E_s when $\Sigma \to 0$. When the system approaches equilibrium and $\Sigma \to 0$, we expect that Δ_b should be proportional to Σ in accordance with a linear response for small deviations from equilibrium[35]. Once equilibrium is reached, the driving force Δ_b equals 0 and $n^+ = n^- = e^{(-E_s/k_\mathrm{B}T)}$. E_b is assumed to depend linearly on Σ, which is the only requirement to get the log-law at constant temperature as shown above

$$E_b(t) = E_s(1 - \Sigma(t)). \tag{4}$$

If we assume that the system is far from equilibrium, we have $\exp(-\frac{\Delta_b}{k_\mathrm{B}T}) \ll 1$ and the evolution of Σ as function of time and temperature is then given by

$$\frac{\mathrm{d}\Sigma(t)}{\mathrm{d}t} = -\nu_0 \Delta_\Sigma \exp\left(-\frac{E_s}{k_\mathrm{B}T(t)}\right) \exp\left(\frac{\Sigma(t)E_s}{k_\mathrm{B}T(t)}\right). \tag{5}$$

The only requirement on Δ_b is that it decreases monotonically upon approaching equilibrium, and Eq. (5) is valid as long as $\Delta_b \gg k_\mathrm{B}T$ for all temperatures at which relaxation is described. For example, to describe relaxation up to 420 K, the condition $\Delta_b > 70\,\mathrm{meV}$ needs to be fulfilled (assuming $1/e^2 \ll 1$).

At constant temperature, this equation can be solved analytically and the resulting evolution of Σ is given by

$$\Sigma(t) = -\frac{k_\mathrm{B}T}{E_s} \log\left(\frac{t+\tau_0}{\tau_1}\right), \tag{6}$$

where $\tau_1 = (k_\mathrm{B}T/\nu_0\Delta_\Sigma E_s)e^{(E_s/k_\mathrm{B}T)}$ and $\tau_0 = \tau_1 e^{(-\Sigma_0 E_s/k_\mathrm{B}T)}$.[36] τ_0 can be interpreted as an incubation time at which the transition to the logarithmic decay occurs, and τ_1 is the time at which equilibrium is reached ($\Sigma \to 0$). When $\tau_0 \ll t \ll \tau_1$, $\Sigma(t)$ exhibits a linear dependence on $\log(t)$. The relaxation is thus predicted to follow a logarithmic law as a function of the annealing time.

V. ELECTRICAL TRANSPORT MODEL

In order to link the structural relaxation described above to electrical observables such as the low-field resistance or more generally the *I*–*V* characteristics of a PCM device, a thorough physics-based description of the electrical transport of the amorphous state is needed. For this, we use a previously developed field- and temperature-dependent model of the electrical conductivity[20]. The model is illustrated schematically in Figure 3. In this multiple-trapping model, the conductivity is calculated based on the transport of charge carriers whose release from their localized states is facilitated by the applied electric field, the Coulombic interactions with neighboring defect centers and temperature.

The activation energy for carrier emission E_a decreases by an amount E_{PF} upon the application of an electric field F (Poole–Frenkel effect)[37–41]. The potential Φ is used to model the interactions between two neighboring defect centers:

$$\Phi(r,\theta,F) = -eFr\cos(\theta) - \frac{\beta^2}{4e}\left(\frac{1}{r} + \frac{1}{s-r}\right) + \frac{\beta^2}{es}.$$

Here, β is the Poole–Frenkel constant, e the electronic charge, θ the direction of escape relative to the direction of the electric field and s the distance between the two defect centers, which we denote as intertrap distance. The energy barrier lowering E_{PF}

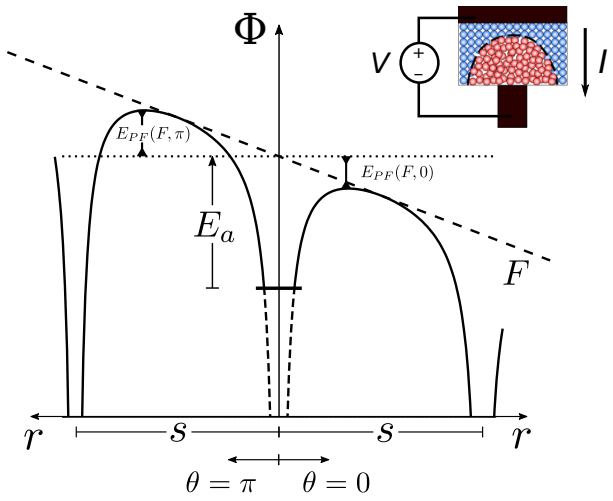

FIG. 3. **Electrical transport model** The field dependence of the free carrier density is described by 3D Poole–Frenkel emission from a two-center Coulomb potential Φ. The applied field F reduces the potential barrier in the direction $\theta = 0$ and increases it along $\theta = \pi$.

due to the Poole–Frenkel effect is calculated for all F and θ by identifying the maximum of this potential over r. Furthermore, the activation energy E_a is assumed to vary with temperature according to

$$E_a = E_{a0} - \xi T^2$$

with $\xi = 0.5 \times 10^{-6}\,\mathrm{eVK}^{-2}$. Such a temperature dependence is inspired by the temperature dependence observed for the optical bandgap of amorphous phase-change materials[28,42,43]. The free carrier density n is then calculated by summing the emission contributions over all directions of escape θ:

$$n(F) = \frac{K}{4\pi}\int_0^{\pi} \exp\left(-\frac{E_a - E_{PF}(F,\theta)}{k_\mathrm{B}T}\right) 2\pi\sin(\theta)d\theta.$$

Finally, the field-dependent electrical conductivity $\sigma(F)$ is calculated as

$$\sigma(F) = e\mu n(F)$$

where μ is the free carrier mobility.

This transport model is capable of describing three regimes of electrical transport observed in amorphous phase-change materials, namely, the ohmic behavior at very low fields, the Poole-type behavior at low to moderate fields and the Poole–Frenkel-type transport at moderate fields. The model was shown to capture the electrical transport in many devices of different dimensions and phase-change materials over a wide temperature range (180 K - 300 K)[20,44]. Even threshold switching in nanoscale PCM devices could be described reasonably well with a simulation solely based on the combination of this subthreshold conduction model with thermal feedback from Joule heating[45], i.e. no additional dependence at high-fields[44] had to be invoked.

VI. LINK BETWEEN ELECTRICAL TRANSPORT AND STRUCTURAL RELAXATION

In sections IV and V, we derived individual descriptions for structural relaxation using the order parameter $\Sigma(t)$ and electrical transport $\sigma(E_{a0}, s)$. In order to find a general quantitative description of resistance drift as a function of temperature and time, we therefore have to establish the link between electrical transport and structural relaxation. Assuming that only E_{a0} and s may potentially vary upon drift[17,20], we therefore need to obtain the functions $E_{a0}(\Sigma(t))$ and $s(\Sigma(t))$. The collective relaxation model leads to a logarithmic law as a function of time at constant temperature. Therefore, we experimentally measured the electrical transport *I–V* characteristics of PCM cells in the RESET (amorphous) state for different annealing times (1000 s and 15 h) at different constant annealing temperatures (250 K, 300 K, 350 K, 400 K). This way we created a highly constrained set of data to experimentally obtain the two quantities E_{a0} and s while all other parameters were held constant. The experiments were conducted on mushroom-type PCM cells fabricated in the 90-nm technology node with doped $Ge_2Sb_2Te_5$ phase-change material (see the experimental section).

The resulting experimental resistance vs. voltage curves corresponding to three such annealing experiments are shown in Figure 4**a**-**c**. It can be seen that the low-field resistance increases with both annealing time and annealing temperature, as it is

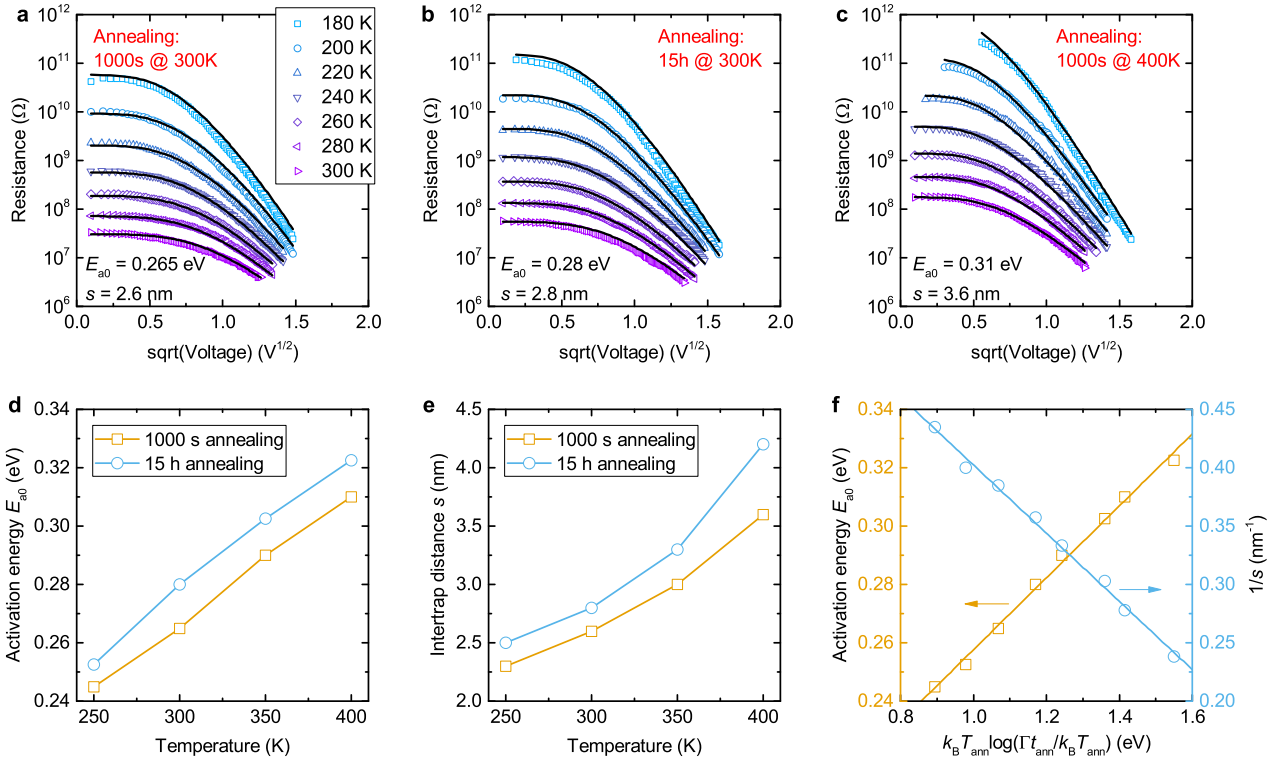

FIG. 4. **Link between electrical transport and structural relaxation a-c**, Experimental resistance vs. voltage curves of RESET state measured from 300 K down to 180 K after annealing. Three annealing conditions are shown, exhibiting higher low-field resistance and stronger voltage dependence for both increasing annealing time and temperature. Fits of the temperature dependent *I–V* characteristics underlying the data in **a-c** using the electrical transport model described in section V (black lines) result in activation energy E_{a0} (**d**) and intertrap distance s (**e**) for different annealing times and temperatures. **f**, E_{a0} and $1/s$ plotted as function of $k_B T_{ann} \log(\Gamma t_{ann}/k_B T_{ann})$, where T_{ann} is the annealing temperature and t_{ann} the annealing time.

typically observed in resistance drift measurements on PCM devices[17,21,42]. It can also be seen that the voltage dependence of the resistance becomes stronger upon annealing.

Figure 4**d** and 4**e** show the values of E_{a0} and s obtained by collectively fitting the resistance vs. voltage curves obtained for each annealing experiment to the electrical transport model introduced in Section V. The activation energy is found to increase linearly with annealing temperature, in agreement with previous experimental measurements[46]. The observed increase of the activation energy upon annealing is consistent with the widening of the optical bandgap seen in amorphous phase-change materials upon annealing[43]. The increase of s upon annealing can be interpreted as being due to the annealing of defects in the bandgap, which presumably are responsible for the Poole–Frenkel-type transport[17,47].

According to the collective relaxation model of Section IV, in particular Eq. (6), all experimental data for different annealing times t_{ann} and temperatures T_{ann} should fall on a single curve when plotted as a function of $k_B T_{ann} \log(\Gamma t_{ann}/k_B T_{ann})$ for a unique value of $\Gamma = E_s \nu_0 \Delta_\Sigma$.[48] This quantity with the dimension of an energy can represent both the effect of longer annealing and of annealing at different temperatures. The good alignment of the data observed in Figure 4**f** for $\Gamma = 2.3 \times 10^{13}$ eVs^{-1} convincingly shows that time-temperature superposition holds for both E_{a0} and s in the experimental range of conditions studied. Time-temperature superposition should be expected if the observed changes in E_{a0} and s indeed arise from structural relaxation[49].

With the annealing kinetics of the PCM cells being well established, E_{a0} and s can now be linked to the order parameter Σ. At constant temperature, for $\tau_0 \ll t \ll \tau_1$, Σ is a linear function of $k_B T \log(\Gamma t/k_B T)$ (see Eq. (6)). Therefore, the experimental results of Figure 4**f** suggest a linear dependence of E_{a0} and $1/s$ with Σ, leading to the following relationships:

$$E_{a0}(t) = E^* - \alpha \Sigma(t) \tag{7}$$

$$s(t) = s_0/\Sigma(t). \tag{8}$$

Here, E^* is the activation energy at equilibrium ($\Sigma = 0$), α is a constant that links a change in $\Sigma(t)$ to a change in $E_{a0}(t)$ and s_0 is a constant that links a change in $\Sigma(t)$ to a change in $s(t)$.

The results from the overall drift model are plotted in Figure 5 along with the experimental data of Figure 4. The solid lines in

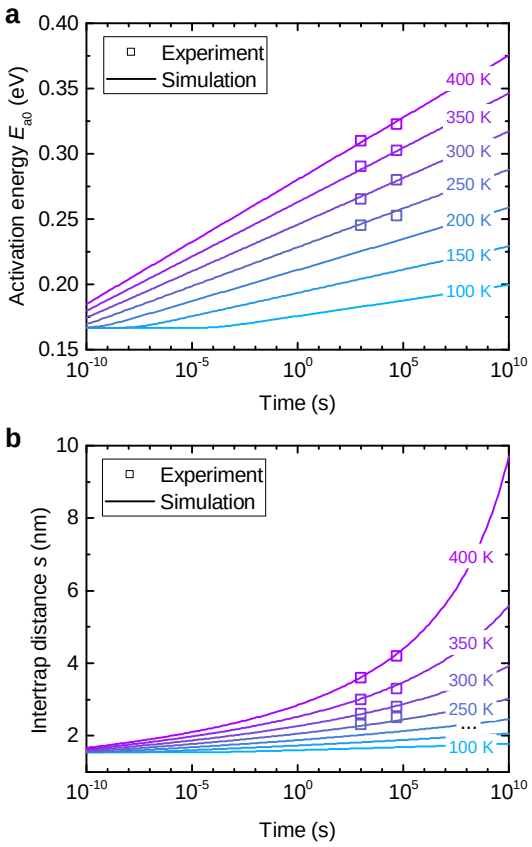

FIG. 5. **Illustration of the drift model** Both E_{a0} and $1/s$ are assumed to vary linearly with the order parameter Σ to constitute the drift model. Those relationships are plotted in **a** and **b** for different ambient temperatures along with the experimental data points of Figure 4.

Figure 5 represent fits to the data, where $\Sigma_0 = 0.9$[50] and $\nu_0\Delta_\Sigma = 10^{13}\,\mathrm{s}^{-1}$ were fixed, and E_s, E^*, α and s_0 were taken as global fit parameters. Good agreement with the data was obtained using $E_s = 2.3\,\mathrm{eV}$, $E^* = 0.415\,\mathrm{eV}$, $\alpha = 0.276\,\mathrm{eV}$ and $s_0 = 1.39\,\mathrm{nm}$. At room temperature, the model yields the logarithmic law from 100 ns (shortest time at which drift has been experimentally observed in PCM cells[33]) up to 10 years (expected retention time of a PCM cell in the RESET state at room temperature[51]).

VII. MODEL VALIDATION

In Section VI, it was shown that collective structural relaxation and field-dependent multiple-trapping electrical transport can be convincingly linked to describe drift of the whole *I–V* characteristics of our PCM cells in the amorphous state. In this section, we want to verify that the model can describe typical experimental resistance drift data collected over an extended range of temperatures and shorter time scales than those previously used to build the model in Section VI. Moreover, we investigate whether the model can also capture drift resulting from the application of a time-dependent temperature profile $T(t)$, using the differential equation (5) to describe the relaxation. Finally, we also investigate how the model can be used to predict the evolution of the resistance distributions of an array of 4k PCM cells.

A. Constant temperature drift

First, constant-temperature low-field resistance drift experiments were conducted over a wide range of temperatures. The PCM cell is programmed to a constant amorphous size at various ambient temperatures (using a technique described in Ref. 51), and the evolution of the low-field resistance R is monitored. The low-field resistance is measured by applying a constant voltage of 0.2 V to the PCM cell. This experiment is conducted from 160 K to 420 K in steps of 20 K. The lower temperature limit is chosen to ensure that the electrical transport does not deviate from the multiple-trapping transport model[28] of Section V and the higher limit to prevent unwanted crystallization. As shown in Figure 6**a**, the experimental data is well captured by the drift

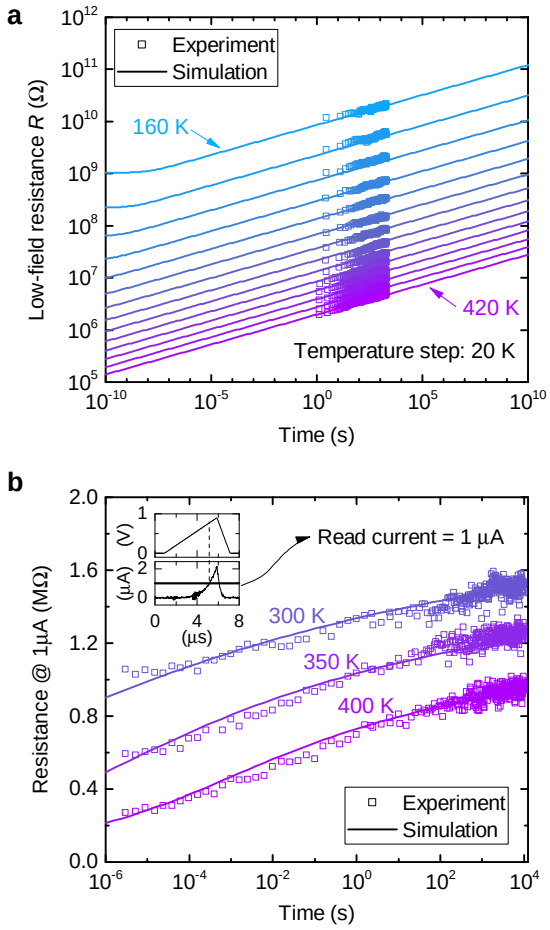

FIG. 6. **Constant temperature drift experiments a**, Low-field resistance drift measured at various temperatures from 160 K to 420 K in steps of 20 K after the PCM cell has been programmed to a constant amorphous size. **b**, High-field resistance drift measured at 300 K, 350 K and 400 K over 10 decades of elapsed time after RESET. The high-field resistance was defined as the resistance of the PCM cell at a fixed current of 1 μA. The inset shows a typical trace of the pulse used to measure the high-field resistance.

model over the whole range of temperatures. The slope of $\log(R)$ vs $\log(t)$ is temperature independent in the experimentally accessible range of time, as commonly observed in resistance drift measurements of phase-change materials[46,52]. This behavior is also predicted by the model because of the linear dependence of E_{a0} on Σ (Eq. (7)). This slope gives the value of the drift exponent ν_R, which can be simply calculated from the model as $\nu_R = \alpha/E_s$ and amounts to $\nu_R = 0.12$ with the parameter values of Section VI.

To test the model on shorter time scales, we performed fast measurements of the high-field resistance starting at 1 μs after RESET over 10 decades in time at temperatures of 300 K, 350 K and 400 K. The high-field resistance is defined as the resistance of the PCM cell at a fixed current of 1 μA (see inset). Defining the high-field resistance in this way allowed us to resolve it accurately with our measurement setup over the entire range of time investigated. The results are shown in Figure 6**b**, and remarkable agreement between model and experiment is obtained over the entire time and temperature range. Note that such a prediction would not be possible without knowing how the *I*–*V* characteristics at high field evolve, because the READ current of 1 μA is beyond the low-field ohmic region of the *I*–*V* curve (see inset).

B. Variable temperature drift

The ultimate test case for the model is a measurement of the full *I*–*V* characteristics of a PCM cell during the application of a time-varying temperature profile. In this case, reversible as well as irreversible effects of temperature on electrical transport need to be tracked correctly upon drift, because structural relaxation is accelerated at higher temperatures. The time-temperature profile shown in Figure 7**a** is applied to the PCM cell after RESET, and the *I*–*V* curves are continuously monitored over time. The

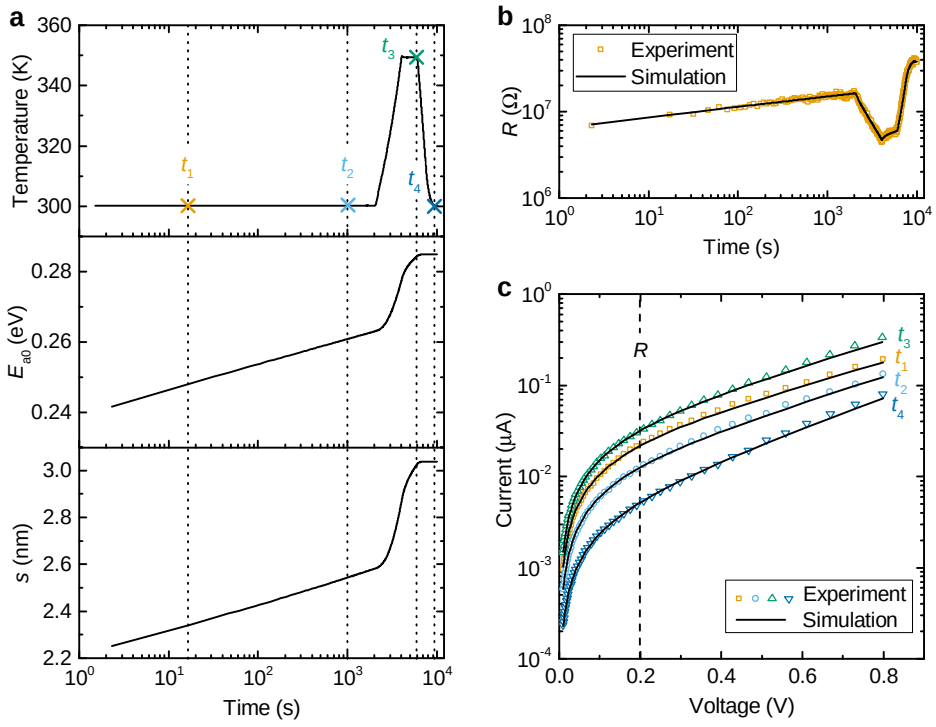

FIG. 7. **Variable temperature *I–V* drift experiment a**, Temperature profile applied to the PCM device and corresponding evolutions of E_{a0} and s obtained from the drift model. **b**, Experimental and simulated evolution of the low-field resistance R. **c**, Experimental and simulated I–V characteristics at four instances in time.

evolution of the low-field resistance R, which corresponds to the ohmic region of the I–V characteristic, is accurately reproduced by the model (Figure 7**b**). Moreover, the I–V curves over the entire voltage range used are accurately predicted by the drift model for the full duration of the experiment (see Figure 7**c**). Note in particular the clear increase of the $\log(I)$ vs V slope after annealing, which is a signature of the increase of s. This increase of s results in a transition from Poole type towards Poole–Frenkel type electrical transport at lower fields, as previously reported on PCM cells that undergo high temperature annealing[17].

C. Array-level drift

Drift variability of PCM devices across an array is arguably the most important problem for multi-level information storage with PCM. Drift variability can cause overlap of the resistance levels used to store the information over time across multiple cells. While techniques such as adaptive detection thresholds can be used to compensate for a global drift effect to reliably detect the stored levels[53], the fact that all cells across an array drift with a different (randomly distributed) exponent ν_R can cause the stored resistance distributions to overlap over time. Therefore, it is of interest to verify if the proposed model can capture the common features observed when monitoring the evolution of the resistance distributions across an array. The evolution of the high-field resistance distributions over time and temperature was measured for an array of 4000 devices in the RESET state. A prototype PCM chip that contains the addressing, readout, and programming circuitry was used for these measurements[54]. The cells were programmed to the RESET state using an iterative procedure[55] to ensure that all cells have approximately the same initial resistance. After programming, the temperature profile shown in Figure 8**a** was applied to the chip and the high-field resistance of the 4000 cells was continuously monitored over time, using a constant read voltage of 0.62 V.

The drift model was used to simulate the evolution of the high-field resistance on 1000 devices. In the simulation, the amorphous thickness (u_a) and drift parameters (α and s_0) were drawn from normal distributions with standard deviation of 5% of the mean values. This way, variability in the initial programmed state is taken into account while the model is used to capture the subsequent evolution of the I–V characteristics of each device with time and temperature. This variability in the initial programmed state is expected to result from both intra- and inter-cell variability. Intra-cell variability is expected because both the thickness of the amorphous region and its internal atomic configuration are never the same after each RESET process.[56] The atoms in the molten state are highly mobile, ensuring that at every RESET a new glass state is formed and this will lead to

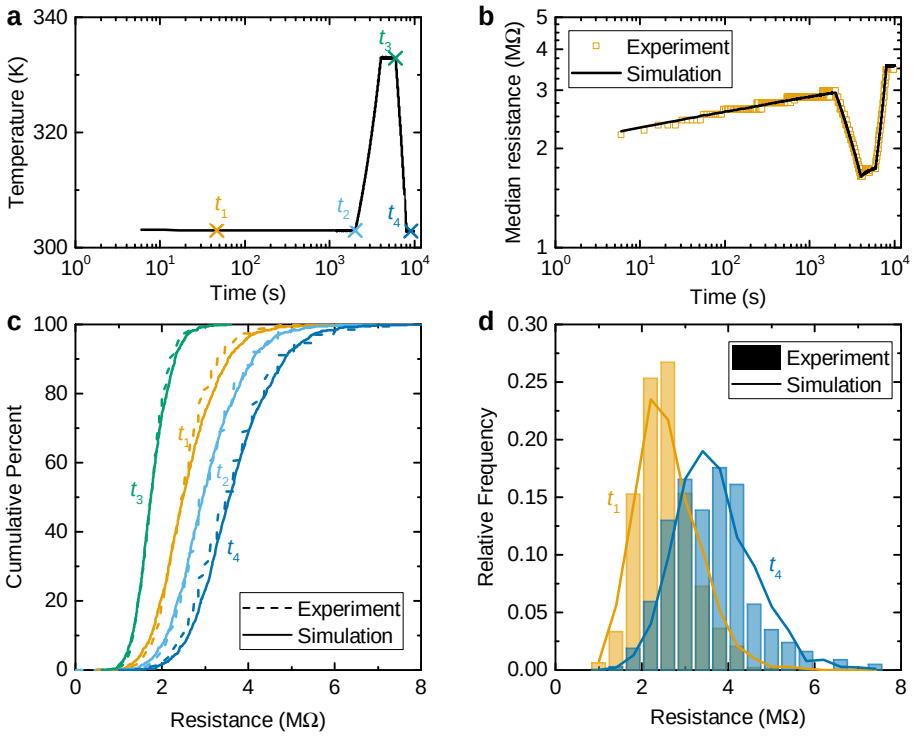

FIG. 8. **Array-level drift experiment** High-field resistance measurements (0.62 V read voltage) were conducted on 4000 devices in the RESET state undergoing changes in the ambient temperature. The drift model was used to simulate the evolution of the high-field resistance on 1000 devices. In the simulation, normal distribution of drift variability and programmed state variability with 5% standard deviation were assumed. **a**, Temperature profile applied to the PCM chip. **b**, Experimental and simulated evolution of the median resistance. **c**, Experimental (dash lines) and simulated (plain lines) cumulative resistance distributions at four instances in time. **d**, Experimental (bars) and simulated (plain lines) resistance histograms before and after annealing.

variability in both u_a and drift. Inter-cell variability, on the other hand, arises predominantly from variability associated with the fabrication process across the array. The distributions simulated this way match very well the experimental distributions of the 4000 devices for the entire experiment, see Figure 8. The model can accurately capture key features[57], such as drift acceleration with increasing temperature, shift of the median values due to temperature changes, and broadening of the distributions upon drift (see Figure 8**d**). The broadening observed after annealing arises because the activation energy and intertrap distance of individual devices relax at slightly different speeds.

VIII. DISCUSSION

Our theoretical as well as experimental results consistently advocate that structural relaxation in phase-change materials is of collective, repetitive nature. We describe such kinetics using a single characteristic activation energy for relaxation that varies with time (Eq. (4)), rather than a distribution of activation energies that gets eroded as in previous works[30]. Our approach naturally gives rise to a logarithmic evolution of the relaxation without the need to assume a wide and flat activation energy spectrum for the relaxation of defects. The collective relaxation model quantifies elegantly the insights from molecular dynamic simulations[27] which indicate that annealing of defective structures occurs via a sequence of activated processes overcoming a changing activation energy. The activation energy for relaxation in Eq. (4) is thus characteristic of a larger ensemble of atoms and not of a single structural defect.

Our experimental data shows that the relaxation in PCM follows the logarithmic law over an extremely wide range of time and temperatures. Hence, describing such kinetics with the Gibbs model based on a distribution of activation energies would require a uniform relaxation energy spectrum spanning more than 15 orders of magnitude in time (see Supplementary Note I), or equivalently several eVs of energy (at least 2 eV[58]). Such a uniformly fine-tuned spectrum over a wide range of time/energy does not appear to be the most physically plausible choice for relaxation in an amorphous material. Such relaxation also cannot be captured by merely using a stretched exponential behavior $\exp[-(t/\tau)^{\gamma}]$ as it is frequently done to describe relaxation in

glasses (see Supplementary Note I)[35,49]. Nonetheless, it is certainly possible to construct an activation energy spectrum of the Gibbs model sufficiently wide and flat, for which the deviation from a log-law can be tuned to be small enough such that the difference to the collective relaxation model is not experimentally accessible. Therefore, as of now we can only claim that the collective relaxation model can provide a more coherent and plausible physical picture. We hope that in the future molecular dynamics simulations will be able to provide reasonable estimates for activation energy spectra that will constrain the Gibbs model sufficiently to resolve this question. Other independent relaxation data not related to electrical transport, such as differential scanning calorimetry or shear modulus data as a function of relaxation[59], could also provide additional insights into the relaxation processes.

The kinetics of repeated rearrangements in the amorphous atomic structure ultimately lead to an increase in the activation energy for electrical transport, E_{a0}, and of the distance between the electronic defect centers, s. These two consequences of structural relaxation are expected to arise from annihilation of defects in the bandgap and the resulting shift of the Fermi level accompanied by a widening of the bandgap due to local reordering[22,25,26,43], both driven by the collective drift dynamics. The empirical link between electrical transport and collective structural relaxation (Eq. (7) and (8)) derived in Section VI is intriguingly simple and enables a quantitative description of a remarkably extensive set of experimental data over a wide range of time (10 orders of magnitude) and temperature (160 K to 420 K). Nonetheless, a better theoretical understanding of Eq. (7) and (8) would be desirable. One avenue to this understanding could be a statistically sufficient set of MD simulations that would provide a quantitative link between the state of relaxation, density of defects in the bandgap and activation energy for conduction. The other approach would be an analytic description of the defect density and activation energy derived from the disordered structure and its evolution upon drift.

The Arrhenius parameters of structural relaxation in amorphous GST have been previously shown to obey the Meyer–Neldel rule (MNR)[58]. The MNR states that the pre-exponential prefactor X_0 of an activated process with activation energy Δ follows the empirical law $X_0 = X_{00} e^{(\Delta/k_B T_{\mathrm{MN}})}$, where T_{MN} is the so-called isokinetic temperature for the process in question, and X_{00} is a constant[58,60]. The MNR is commonly understood to result from the entropy of combining multiple excitations (or fluctuations) in the thermal reservoir available for the kinetic processes[60]. We do not see any direct conflict between the MNR and the collective relaxation model proposed in this paper, and hence MNR could be included in the prefactor ν_0 of the rates of relaxation events (n^+ and n^-) in our model for a more refined picture of the relaxation. We do observe evidence of the MNR in the experimental resistance drift data of Figure 6**a**, however the resulting isokinetic temperature $T_{\mathrm{MN}} = 1639$ K is much higher than the value of 760 K previously reported for amorphous $Ge_2Sb_2Te_5$[58] (see Supplementary Note II). This discrepancy could be potentially explained by the different material, doped $Ge_2Sb_2Te_5$, used in our devices.

The high value of $E_s = 2.3$ eV obtained from the fit in Figure 5 is consistent with the fact that no saturation of the temporal evolution of the electrical conductivity of phase-change materials has yet been observed experimentally. According to the model, such saturation would happen at time τ_1, which depends exponentially on E_s and takes values much larger than the typical crystallization time of this material at a given temperature[51]. This shows that in most practical cases, no saturation of structural relaxation is expected to be observable experimentally at least in the material studied here. It is also interesting that E_s, the upper limit of activation energy for structural relaxation in our model, is lower, but relatively close, to the activation energy for crystal growth of 3.01 eV reported for the same material[51]. Indeed, both relaxation towards the ideal glass as well as crystallization lead to the same local rearrangements[22,25]. Crystallization has the additional constraint that the local unit cells are also in order relative to each other. Therefore, it is not surprising that the activation energies are similar but slightly higher in the case of crystallization.

Moreover, the high value of $\Sigma_0 = 0.9$ needed to describe the experimental data can be interpreted as a direct consequence of the high quench rates (on the order of 10^{11} Ks^{-1}) resulting from the RESET operation, which create a highly stressed amorphous state. The fact that structural relaxation is observed already at microsecond time scales and at temperatures much lower than room temperature clearly confirms that the state initially created by the melt-quench process is far away from equilibrium (Σ_0 must be close to 1).

Finally, it is worth asking whether the findings reported here are applicable to other phase-change materials than the doped $Ge_2Sb_2Te_5$ used in this study. In a previous work, we showed that our model can also capture the structural relaxation in doped GeTe PCM cells, albeit with different parameters[23]. Moreover, almost all phase-change materials studied to date, even when composed of a single element (antimony)[61], show similar resistance drift behavior that can be described using Eq. (1), although the drift exponent ν_R can differ from one material to another[43,62]. Those findings suggest that the general drift behavior in phase-change materials is fairly universal. Different materials will have different electrical transport properties and may relax at different speeds, but the overall "$\log(t)$" drift dynamics and their dependence on temperature are expected to hold no matter what material is used.

IX. CONCLUSION

The root cause of resistance drift in PCM devices is the spontaneous structural relaxation of the amorphous state created via the melt-quench process. This amorphous state over time evolves towards an energetically more favorable ideal glass state.

First-principles calculations on amorphous GeTe indicate a direct correlation between the resistance increase and annihilation of defects responsible for localized electronic states in the band gap, which occurs via a series of collective rearrangements of the defective structural complexes. Based on this insight, we propose a collective relaxation model to describe the kinetics of structural relaxation in amorphous phase-change materials. As opposed to previous approaches based on the relaxation model by Gibbs[31], a logarithmic evolution of the relaxation is obtained over a wide range of time and temperature without the need to assume a rather wide and flat activation energy spectrum for the relaxation of defects. An intriguingly simple link between electrical transport and structural relaxation is introduced and validated over an extensive range of experimental conditions. For the first time, a model can consistently predict the changes observed in the *I–V* characteristics of PCM cells over time and temperature. Constant and variable temperature drift measurements performed on PCM cells over a wide range of time (10 decades) and temperatures (160 - 420 K) are well captured by the model. Moreover, the model can capture the evolution of the resistance distributions in an array of PCM cells by introducing variability in the size of the initially programmed amorphous region as well as in the parameters governing drift. This work presents a quantitatively accurate and comprehensive description of resistance drift in PCM devices, and is expected to be relevant for emerging application areas such as storage-class memory, neuromorphic computing and computational memory.

X. EXPERIMENTAL SECTION

Experimental details: Experiments were conducted using mushroom-type PCM cells fabricated in the 90-nm technology node, with the bottom electrode created via sub-lithographic key-hole process[63]. The phase-change material is doped $Ge_2Sb_2Te_5$. The bottom electrode has a radius of ~ 20 nm and a length of ~ 65 nm. The phase-change material is ~ 100 nm thick and extends to the top electrode, whose radius is ~ 100 nm. The device is operated with an on-chip series resistor of ~ 5 kΩ.

For the experiments of Section VI and the low-field resistance measurements of Section VII A, a JANIS ST-500-2-UHT cryogenic probing station that operates from 77 K to 400 K and offers a temperature stability of less than 50 mK was used to perform the measurements. A high-precision Keithley 2636B SMU was used for DC voltage outputs and for measuring the corresponding current at the sample, with a resolution of ~ 0.1 pA.

For the high-field resistance measurements of Section VII A and the experiments of Section VII B, the ambient temperature was varied using a custom-made heating stage made of invar. The temperature was measured using a thermocouple inserted into the invar block and controlled via a Eurotherm temperature controller. The temperature on top of the PCM chip was further calibrated using an Omega silicon diode sensor. A Keithley 2400 SMU was used for DC voltage outputs and for measuring the corresponding current at the sample. For the high-field resistance measurements, AC voltage outputs were given by a Agilent 81150A Pulse Function Arbitrary Generator and the corresponding cell voltage and current were measured with a Tektronix DPO5104B digital oscilloscope. The current was amplified by an operational amplifier circuit with a total gain of ~ 9.2 prior to measurement.

Annealing experiments of Section VI: First, an amorphous region is created with a RESET current of 800 μA. Thereafter, the PCM cell is annealed at a certain temperature for a certain time duration. After annealing, the *I–V* characteristics are measured at different temperatures down to 180 K. This set of experiments was repeated eight times over annealing temperatures varying from 250 K to 400 K in steps of 50 K and annealing times of 1000 s and 15 h. The resistance is calculated as the applied voltage divided by the measured current. The resistance vs. voltage curves obtained after each annealing experiment are then collectively fitted to the electrical transport model introduced in Section V. We assume that the applied electric field is $F = V/u_a$, where V is the applied voltage on the cell and u_a an effective amorphous thickness roughly equal to the smallest pathway of conduction through the amorphous region. Moreover, the device area used for the calculation of the current is assumed to be πr_{BE}^2, where r_{BE} is an effective bottom-electrode radius. It has been shown that introducing these two effective parameters allows the mushroom cell geometry to be well approximated by a cylindrical geometry of radius r_{BE} with a uniform field applied over u_a[64]. It is found that only the activation energy E_{a0} and the intertrap distance s must be modified at different degrees of relaxation to achieve good fits. The parameters related to the cell geometry are fixed to $u_a = 12.5$ nm and $r_{\mathrm{BE}} = 20$ nm. The remaining parameters are fixed to the values found in Ref. 20.

SUPPORTING INFORMATION

Supporting information is available from the Wiley Online Library or from the author.

ACKNOWLEDGEMENTS

We are grateful to U. Egger and W. Häberle for technical assistance. We would also like to thank our colleagues at IBM T. J. Watson Research Center in particular M. BrightSky for providing the PCM cells used in this work. A. Sebastian, D. Krebs

and M. Salinga acknowledge funding from the DIASPORA project (Ref. 610781) of the FP7-IAPP Marie Curie Action by the European Commission. A. Sebastian and M. Salinga acknowledge funding from the European Research Council grants PROJESTOR (Ref. 682675) and NEUROMORPH (Ref. 640003), respectively. M. Salinga also acknowledges funding from the German Science Foundation (DFG) through the Collaborative Research Center NANOSWITCHES (SFB 917). Finally, we would like to acknowledge fruitful discussions with M. Stanislavjevic, N. Papandreou, M. Kaes, M. Ruetten and W. Koelmans. We would also like to thank H. Pozidis, E. Eleftheriou and A. Curioni for managerial support.

KEYWORDS

Phase-change materials, nonvolatile memory, structural relaxation, kinetics

REFERENCES

[1]H.-S. P. Wong and S. Salahuddin, "Memory leads the way to better computing," Nature nanotechnology **10**, 191–194 (2015).
[2]S. W. Fong, C. M. Neumann, and H.-S. P. Wong, "Phase-change memory – towards a storage-class memory," IEEE Transactions on Electron Devices **64**, 4374–4385 (2017).
[3]S. Raoux, G. W. Burr, M. J. Breitwisch, C. T. Rettner, Y.-C. Chen, R. M. Shelby, M. Salinga, D. Krebs, S.-H. Chen, H.-L. Lung, and C. H. Lam, "Phase-change random access memory: A scalable technology," IBM Journal of Research and Development **52**, 465–479 (2008).
[4]G. W. Burr, M. J. Brightsky, A. Sebastian, H. Y. Cheng, J. Y. Wu, S. Kim, N. E. Sosa, N. Papandreou, H. L. Lung, H. Pozidis, E. Eleftheriou, and C. H. Lam, "Recent progress in phase-change memory technology," IEEE Journal on Emerging and Selected Topics in Circuits and Systems **6**, 146–162 (2016).
[5]N. Papandreou, H. Pozidis, A. Pantazi, A. Sebastian, M. Breitwisch, C. Lam, and E. Eleftheriou, "Programming algorithms for multilevel phase-change memory," in *Proc. International Symposium on Circuits and Systems (ISCAS)* (2011) pp. 329–332.
[6]A. Sebastian, M. Le Gallo, W. Koelmans, N. Papandreou, H. Pozidis, and E. Eleftheriou, "Multi-level storage in phase-change memory devices," in *Proceedings of the EPCOS* (2016).
[7]C. D. Wright, P. Hosseini, and J. A. V. Diosdado, "Beyond von-neumann computing with nanoscale phase-change memory devices," Advanced Functional Materials **23**, 2248–2254 (2013).
[8]P. Hosseini, A. Sebastian, N. Papandreou, C. D. Wright, and H. Bhaskaran, "Accumulation-based computing using phase-change memories with FET access devices," IEEE Electron Device Letters **36**, 975–977 (2015).
[9]M. Le Gallo, A. Sebastian, R. Mathis, M. Manica, H. Giefers, T. Tuma, C. Bekas, A. Curioni, and E. Eleftheriou, "Mixed-precision in-memory computing," Nature Electronics **1**, 246 (2018).
[10]A. Sebastian, T. Tuma, N. Papandreou, M. Le Gallo, L. Kull, T. Parnell, and E. Eleftheriou, "Temporal correlation detection using computational phase-change memory," Nature Communications **8**, 1115 (2017).
[11]M. Le Gallo, A. Sebastian, G. Cherubini, H. Giefers, and E. Eleftheriou, "Compressed sensing recovery using computational memory," in *Proc. IEEE International Electron Devices Meeting (IEDM)* (2017) pp. 28.3.1–28.3.4.
[12]G. W. Burr, R. M. Shelby, A. Sebastian, S. Kim, S. Kim, S. Sidler, K. Virwani, M. Ishii, P. Narayanan, A. Fumarola, *et al.*, "Neuromorphic computing using non-volatile memory," Advances in Physics: X **2**, 89–124 (2017).
[13]G. W. Burr, R. M. Shelby, S. Sidler, C. di Nolfo, J. Jang, I. Boybat, R. S. Shenoy, P. Narayanan, K. Virwani, E. U. Giacometti, B. N. Kurdi, and H. Hwang, "Experimental demonstration and tolerancing of a large-scale neural network (165 000 synapses) using phase-change memory as the synaptic weight element," IEEE Transactions on Electron Devices **62**, 3498–3507 (2015).
[14]T. Tuma, A. Pantazi, M. Le Gallo, A. Sebastian, and E. Eleftheriou, "Stochastic phase-change neurons," Nature nanotechnology **11**, 693 (2016).
[15]D. Ielmini, S. Lavizzari, D. Sharma, and A. L. Lacaita, "Physical interpretation, modeling and impact on phase change memory (PCM) reliability of resistance drift due to chalcogenide structural relaxation," in *Proc. IEEE International Electron Devices Meeting (IEDM)* (IEEE, 2007) pp. 939–942.
[16]M. Boniardi, A. Redaelli, A. Pirovano, I. Tortorelli, D. Ielmini, and F. Pellizzer, "A physics-based model of electrical conduction decrease with time in amorphous $Ge_2Sb_2Te_5$," Journal of Applied Physics **105**, 084506 (2009).
[17]D. Ielmini, D. Sharma, S. Lavizzari, and A. Lacaita, "Reliability impact of chalcogenide-structure relaxation in phase-change memory (PCM) cells, part I: Experimental study," IEEE Trans. Electron Devices **56**, 1070–1077 (2009).
[18]M. Rizzi, A. Spessot, P. Fantini, and D. Ielmini, "Role of mechanical stress in the resistance drift of $Ge_2Sb_2Te_5$ films and phase change memories," Applied Physics Letters **99**, 223513 (2011).
[19]P. Fantini, S. Brazzelli, E. Cazzini, and A. Mani, "Band gap widening with time induced by structural relaxation in amorphous $Ge_2Sb_2Te_5$ films," Applied Physics Letters **100**, 013505 (2012).
[20]M. Le Gallo, M. Kaes, A. Sebastian, and D. Krebs, "Subthreshold electrical transport in amorphous phase-change materials," New Journal of Physics **17**, 093035 (2015).
[21]A. Sebastian, D. Krebs, M. Le Gallo, H. Pozidis, and E. Eleftheriou, "A collective relaxation model for resistance drift in phase change memory cells," in *Proc. IEEE International Reliability Physics Symposium (IRPS)* (2015) pp. MY.5.1–MY.5.6.
[22]F. Zipoli, D. Krebs, and A. Curioni, "Structural origin of resistance drift in amorphous GeTe," Physical Review B **93**, 115201 (2016).
[23]M. Le Gallo, A. Sebastian, D. Krebs, M. Stanisavljevic, and E. Eleftheriou, "The complete time/temperature dependence of I-V drift in PCM devices," in *Proc. IEEE International Reliability Physics Symposium (IRPS)* (2016) pp. MY–1–1–MY–1–6.
[24]F. Zipoli and A. Curioni, "A theoretical approach to modeling the amorphous phase of GeTe for PCM," in *Proceedings of the EPCOS* (2013).
[25]J. Y. Raty, W. Zhang, J. Luckas, C. Chen, R. Mazzarello, C. Bichara, and M. Wuttig, "Aging mechanisms in amorphous phase-change materials," Nature communications **6**, 7467 (2015).
[26]S. Gabardi, S. Caravati, G. Sosso, J. Behler, and M. Bernasconi, "Microscopic origin of resistance drift in the amorphous state of the phase-change compound GeTe," Physical Review B **92**, 054201 (2015).
[27]F. Zipoli and A. Curioni, "Reactive potential for the study of phase-change materials: GeTe," New Journal of Physics **15**, 123006 (2013).

[28] D. Krebs, T. Bachmann, P. Jonnalagadda, L. Dellmann, and S. Raoux, "Changes in electrical transport and density of states of phase change materials upon resistance drift," New Journal of Physics **16**, 043015 (2014).

[29] D. Ielmini, S. Lavizzari, D. Sharma, and A. L. Lacaita, "Temperature acceleration of structural relaxation in amorphous $Ge_2Sb_2Te_5$," Applied Physics Letters **92**, 193511 (2008).

[30] S. Lavizzari, D. Ielmini, D. Sharma, and A. L. Lacaita, "Reliability impact of chalcogenide-structure relaxation in phase-change memory (PCM) cells part II: physics-based modeling," IEEE Trans. Electron Devices **56**, 1078–1085 (2009).

[31] M. Gibbs, J. Evetts, and J. Leake, "Activation energy spectra and relaxation in amorphous materials," Journal of Materials Science **18**, 278–288 (1983).

[32] In case of bi-molecular relaxation, Eq. (2) becomes $\mathrm{d}q(E)/\mathrm{d}t = -\nu(E)q(E)^2$.

[33] D. Ielmini, A. Lacaita, and D. Mantegazza, "Recovery and drift dynamics of resistance and threshold voltages in phase-change memories," IEEE Trans. Electron Devices **54**, 308–315 (2007).

[34] D. Kuhlmann, "Zur theorie der nachwirkungserscheinungen," Zeitschrift für Physik A Hadrons and Nuclei **124**, 468–481 (1948).

[35] A. Knoll, D. Wiesmann, B. Gotsmann, and U. Duerig, "Relaxation kinetics of nanoscale indents in a polymer glass," Physical Review Letters **102**, 117801 (2009).

[36] Because $\Sigma(0) = \Sigma_0$ by definition, we look for a solution to Eq. (5) of the form $\Sigma(t) = A\log\left(\frac{t+\tau_0}{\tau_1}\right)$. Inserting this solution into Eq. (5) for constant temperature $T(t) = T$ yields $\frac{A}{t+\tau_0} = -\nu_0\Delta_\Sigma \exp\left(-\frac{E_s}{k_\mathrm{B}T}\right)\left(\frac{t+\tau_0}{\tau_1}\right)^{AE_s/k_\mathrm{B}T}$ which has for solution $A = -\frac{k_\mathrm{B}T}{E_s}$ and $\tau_1 = -\frac{A}{\nu_0\Delta_\Sigma}\exp\left(\frac{E_s}{k_\mathrm{B}T}\right)$. Using $\Sigma(0) = \Sigma_0$ gives $A\log\left(\frac{\tau_0}{\tau_1}\right) = \Sigma_0$, therefore $\tau_0 = \tau_1\exp\left(\frac{\Sigma_0}{A}\right)$.

[37] R. M. Hill, "Poole-Frenkel conduction in amorphous solids," Philosophical Magazine **23**, 59–86 (1971).

[38] D. Ielmini and Y. Zhang, "Analytical model for subthreshold conduction and threshold switching in chalcogenide-based memory devices," Journal of Applied Physics **102**, 054517 (2007).

[39] G. B. Beneventi, L. Guarino, M. Ferro, and P. Fantini, "Three-dimensional Poole-Frenkel analytical model for carrier transport in amorphous chalcogenides," Journal of Applied Physics **113**, 044506 (2013).

[40] M. Ieda, G. Sawa, and S. Kato, "A consideration of Poole-Frenkel effect on electric conduction in insulators," Journal of Applied Physics **42**, 3737–3740 (1971).

[41] J. L. Hartke, "The three-dimensional Poole-Frenkel effect," Journal of Applied Physics **39**, 4871–4873 (1968).

[42] J. L. M. Oosthoek, D. Krebs, M. Salinga, D. J. Gravesteijn, G. A. M. Hurkx, and B. J. Kooi, "The influence of resistance drift on measurements of the activation energy of conduction for phase-change material in random access memory line cells," Journal of Applied Physics **112**, 084506 (2012).

[43] M. Rütten, M. Kaes, A. Albert, M. Wuttig, and M. Salinga, "Relation between bandgap and resistance drift in amorphous phase change materials," Scientific Reports **5**, 17362 (2015).

[44] M. Kaes, M. Le Gallo, A. Sebastian, M. Salinga, and D. Krebs, "High-field electrical transport in amorphous phase-change materials," Journal of Applied Physics **118**, 135707 (2015).

[45] M. Le Gallo, A. Athmanathan, D. Krebs, and A. Sebastian, "Evidence for thermally assisted threshold switching behavior in nanoscale phase-change memory cells," Journal of Applied Physics **119**, 025704 (2016).

[46] D. Krebs, R. M. Schmidt, J. Klomfass, J. Luckas, G. Bruns, C. Schlockermann, M. Salinga, R. Carius, and M. Wuttig, "Impact of DoS changes on resistance drift and threshold switching in amorphous phase change materials," Journal of Non-Crystalline Solids **358**, 2412 – 2415 (2012).

[47] M. Kaes and M. Salinga, "Impact of defect occupation on conduction in amorphous $Ge_2Sb_2Te_5$," Scientific Reports **6**, 31699 (2016).

[48] For $t \gg \tau_0$, Eq. (6) simplifies to $\Sigma(t) = 1 - \frac{k_\mathrm{B}T}{E_s}\log\left(\frac{E_s\nu_0\Delta_\Sigma t}{k_\mathrm{B}T}\right) = 1 - \frac{k_\mathrm{B}T}{E_s}\log\left(\frac{\Gamma t}{k_\mathrm{B}T}\right)$ where $\Gamma = E_s\nu_0\Delta_\Sigma$.

[49] C. A. Angell, K. L. Ngai, G. B. McKenna, P. F. McMillan, and S. W. Martin, "Relaxation in glassforming liquids and amorphous solids," Journal of Applied Physics **88**, 3113–3157 (2000).

[50] A precise value of Σ_0 could not be derived from our data because τ_0 was not accessible in our range of experimental conditions. Hence, the value of $\Sigma_0 = 0.9$ was chosen such that the log-law starts from approximately 100 ns[33] at 160 K, which is the lowest temperature at which we measured resistance drift in our devices.

[51] A. Sebastian, M. Le Gallo, and D. Krebs, "Crystal growth within a phase change memory cell," Nature Communications **5**, 4314 (2014).

[52] M. Boniardi and D. Ielmini, "Physical origin of the resistance drift exponent in amorphous phase change materials," Applied Physics Letters **98**, 243506 (2011).

[53] N. Papandreou, H. Pozidis, T. Mittelholzer, G. Close, M. Breitwisch, C. Lam, and E. Eleftheriou, "Drift-tolerant multilevel phase-change memory," in *Proc. International Memory Workshop (IMW)* (2011) pp. 1–4.

[54] G. Close, U. Frey, M. Breitwisch, H. Lung, C. Lam, C. Hagleitner, and E. Eleftheriou, "Device, circuit and system-level analysis of noise in multi-bit phase-change memory," in *2010 IEEE International Electron Devices Meeting (IEDM)* (IEEE, 2010) pp. 29–5.

[55] N. Papandreou, H. Pozidis, A. Pantazi, A. Sebastian, M. Breitwisch, C. Lam, and E. Eleftheriou, "Programming algorithms for multilevel phase-change memory," in *2011 IEEE International Symposium on Circuits and Systems* (IEEE, 2011) pp. 329–332.

[56] M. Le Gallo, T. Tuma, F. Zipoli, A. Sebastian, and E. Eleftheriou, "Inherent stochasticity in phase-change memory devices," in *46th European Solid-State Device Research Conference (ESSDERC)* (IEEE, 2016) pp. 373–376.

[57] M. Stanisavljevic, A. Athmanathan, N. Papandreou, H. Pozidis, and E. Eleftheriou, "Phase-change memory: Feasibility of reliable multilevel-cell storage and retention at elevated temperatures," in *Proc. IEEE International Reliability Physics Symposium (IRPS)* (2015) pp. 5B.6.1–5B.6.6.

[58] D. Ielmini and M. Boniardi, "Common signature of many-body thermal excitation in structural relaxation and crystallization of chalcogenide glasses," Applied Physics Letters **94**, 091906 (2009).

[59] A. Tsyplakov, Y. P. Mitrofanov, A. Makarov, G. Afonin, and V. Khonik, "Determination of the activation energy spectrum of structural relaxation in metallic glasses using calorimetric and shear modulus relaxation data," Journal of Applied Physics **116**, 123507 (2014).

[60] G. Boisvert, L. J. Lewis, and A. Yelon, "Many-body nature of the Meyer-Neldel compensation law for diffusion," Physical review letters **75**, 469 (1995).

[61] M. Salinga, B. Kersting, I. Ronneberger, V. P. Jonnalagadda, X. Thang Vu, M. Le Gallo, I. Giannopoulos, O. Cojocaru-Mirédin, R. Mazzarello, and A. Sebastian, "Monoatomic phase change memory," Nature Materials (2018), in press.

[62] M. Wimmer, M. Kaes, C. Dellen, and M. Salinga, "Role of activation energy in resistance drift of amorphous phase change materials," Frontiers in Physics **2**, 75 (2014).

[63] M. Breitwisch, T. Nirschl, C. F. Chen, Y. Zhu, M. H. Lee, M. Lamorey, G. W. Burr, E. Joseph, A. Schrott, J. B. Philipp, R. Cheek, T. D. Happ, S. H. Chen, S. Zaidi, P. Flaitz, J. Bruley, R. Dasaka, B. Rajendran, S. Rossnagel, M. Yang, Y. C. Chen, R. Bergmann, H. L. Lung, and C. Lam, "Novel lithography-independent pore phase change memory," in *Proc. IEEE Symposium on VLSI Technology* (2007) pp. 100–101.

[64] A. Sebastian, N. Papandreou, A. Pantazi, H. Pozidis, and E. Eleftheriou, "Non-resistance-based cell-state metric for phase-change memory," Journal of Applied Physics **110**, 084505 (2011).